Letter

Topology of three-dimensional Dirac semimetals and quantum spin Hall systems without gapless edge modes

Alexander C. Tyner[1,*] Shouvik Sur[2,*] Danilo Puggioni[3] James M. Rondinelli[1,3,4] and Pallab Goswami[1,2]

[1]*Graduate Program in Applied Physics, Northwestern University, Evanston, Illinois 60208,USA*
[2]*Department of Physics and Astronomy, Northwestern University, Evanston, Illinois 60208, USA*
[3]*Department of Materials Science and Engineering, Northwestern University, Illinois 60208, USA*
[4]*Northwestern Argonne Institute for Science and Engineering, Evanston, Illinois 60208, USA*

(Received 14 January 2022; revised 20 November 2022; accepted 28 November 2022; published 13 February 2023)

The quantum spin Hall states are usually expected to possess gapless, helical edge modes. We show that the generic, n-fold-symmetric, momentum planes of three-dimensional, stable Dirac semimetals, which are orthogonal to the direction of nodal separation are examples of generalized quantum spin Hall systems, that possess quantized, spin or relative Chern numbers as bulk topological invariants, and gapped edge modes. We demonstrate these planes and the celebrated Bernevig-Zhang-Hughes model support identical quantized, non-Abelian Berry flux of magnitude 2π. Hence, they display identical quantized, topological response such as spin-charge separation and pumping of one Kramers-pair or $SU(2)$ doublet, when probed with a magnetic flux tube. The Dirac points are identified as unit-strength, monopoles of $SO(5)$ Berry connection, describing topological phase transitions between generalized quantum spin Hall and trivial insulators. Our work identifies precise bulk invariant and quantized response of Dirac semimetals, which are not diagnosed by nested Wilson loops and filling anomaly of corner-localized-states, and shows that many two-dimensional higher-order topological insulators can be understood as generalized quantum spin Hall systems.

DOI: 10.1103/PhysRevResearch.5.L012019

Introduction. The stable, three-dimensional, Dirac semimetals (DSM) arising from accidental linear touching between two Kramers-degenerate bands at isolated points in the Brillouin zone (BZ) are experimentally relevant examples of gapless topological states [1–19]. The Dirac points of such systems, occurring along an n-fold axis of rotation are protected by the combined $\mathcal{PT}$ and the n-fold, discrete, rotational ($\mathcal{C}_n$) symmetries, with $n = 3, 4, 6$ [1,2], where $\mathcal{P}$ and $\mathcal{T}$ represent space-inversion/parity ($\mathcal{P}$) and time-reversal ($\mathcal{T}$) symmetries, respectively. Several materials like Na_3Bi [1,20–23], Cd_3As_2 [2,24–29], $PdTe_2$ [30], β'-PtO_2 [16,19], VAl_3 [11], β-CuI [13], KMgBi [12,19], $PtBi_2$ [31], and the magnetoelectric compound FeSn [9,32] can host such Dirac points. Despite intensive theoretical research on stable DSMs for almost ten years [1–16,18,19], their bulk topological invariants are still unknown.

The simplest version of DSMs can be obtained by stacking of Bernevig-Hughes-Zhang (BHZ) model [33] of quantum spin Hall (QSH) effect along the direction of nodal separation or the $\mathcal{C}_n$ axis. Since the BHZ model is a first-order topological insulator (FOTI), supporting helical edge modes, the resulting DSM exhibits loci of zero-energy surface states, also known as the helical Fermi arcs. The total number of zero modes is equal to the total QSH conductivity of DSMs, determined by $\Delta k_D/\pi$, where Δk_D is the distance between the bulk Dirac nodes. The spectroscopic and transport data of many stable DSMs are usually interpreted based on the existence of helical Fermi arcs [20–30,32].

However, recent theoretical works [7,17–19] have shown that the generic, n-fold planes of DSMs are not described by the BHZ model possessing $U(1)$ spin-conservation law, or closely related $\mathbb{Z}_2$ FOTIs [34]. Away from the mirror planes, various crystalline-symmetry-preserving perturbations can gap out the helical edge modes. The topological properties of these planes were not addressed in Refs. [3,4], as the authors focused only on the difference between high-symmetry planes. Using K-theory analysis, the generic planes were found to be topologically trivial [7]. Subsequently, various groups [17–19,35] have identified these planes as higher-order, topological insulators (HOTI) [36]. The distinction between FOTI and HOTI is established by computing the nested Wilson loops of $SU(2)$ Berry connection for the occupied valence bands under periodic boundary conditions and the filling anomaly due to corner-localized-states under $\mathcal{C}_n$-symmetric open boundary conditions. *However, such analysis does not address the presence or absence of spin-Chern number [37,38] as a bulk topological invariant. The primary goal of this Letter is to compute and probe the spin Chern number of generic planes of DSMs.*

What happens to the QSH effect of the BHZ model, when the $U(1)$ spin-conservation law and the helical edge modes

*These authors contributed equally to this work.

get destroyed by crystal-symmetry-preserving perturbations? This question has intrigued condensed matter physicists since 2006, leading to the formulation of the spin-Chern number in terms of generalized twisted boundary conditions [37,38]. Qi *et al.* studied a C_4-symmetric model of QSH insulators, possessing gapped edge modes [38], which is topologically equivalent to the generic planes of C_4-symmetric DSMs. Using generalized twisted boundary conditions, they argued the spin Chern number to be ± 4. Recently, this work has inspired Song *et al.* [39] to categorize the spectral flow of fragile topological insulators, lacking Kramers degeneracy. However, the important question, whether the spin Chern number of generic planes of Kramers-degenerate DSMs is ± 2 or ± 4, has not been addressed. If the spin Chern number is ± 2 (± 4), Dirac points would act as unit-strength (double) monopoles. In this work, we perform second homotopy classification of the non-Abelian Berry connection to show that the spin Chern number is ± 2, and Dirac points are unit strength monopoles. The analysis of momentum space invariant will be substantiated by probing real-space topological response with a magnetic flux tube.

Challenge toward topological classification. The minimal model of a pair of twofold, Kramers-degenerate bands of $\mathcal{PT}$ symmetric systems is described by the Hamiltonian $H = \sum_{\boldsymbol{k}} \Psi^\dagger(\boldsymbol{k})\hat{H}(\boldsymbol{k})\Psi(\boldsymbol{k})$, where $\Psi(\boldsymbol{k})$ is a four-component spinor, and the Bloch Hamiltonian operator can be written as [40–43] $\hat{H}(\boldsymbol{k}) = N_0(\boldsymbol{k})\mathbb{1} + \sum_{j=1}^{5} N_j(\boldsymbol{k})\Gamma_j$. The magnitude of $O(5)$ vector $\boldsymbol{N}(\boldsymbol{k})$ controls the spectral gap between conduction and valence bands, $N_0(\boldsymbol{k})$ describes particle-hole anisotropy, and Γ_j are five, mutually anticommuting, 4×4 matrices, such that $\{\Gamma_i, \Gamma_j\} = 2\delta_{ij}$. Since the projection operators for conduction and valence bands are given by $\hat{P}_\pm(\boldsymbol{k}) = \frac{1}{2}(\mathbb{1} \pm \hat{\boldsymbol{N}}(\boldsymbol{k}) \cdot \boldsymbol{\Gamma})$, the topology of Bloch wave functions is determined by the unit O(5) vector $\hat{\boldsymbol{N}}(\boldsymbol{k}) = \boldsymbol{N}(\boldsymbol{k})/|\boldsymbol{N}(\boldsymbol{k})|$, representing the coset space $SO(5)/SO(4) = S^4$, where S^4 is the unit, four sphere. On the fermionic spinor $\Psi(\boldsymbol{k})$, the action of $SO(5)$ and $SO(4)$ groups are realized in terms of their double cover groups $Spin(5)$ and $Spin(4) = SU(2) \times SU(2)$, respectively. Therefore, the diagonalizing matrix of the Bloch Hamiltonian belongs to the coset space $\frac{SO(5)}{SO(4)} = \frac{Spin(5)}{Spin(4)} = S^4$, and the gauge group for the intraband Berry connection is given by $Spin(4) = SU(2) \times SU(2)$.

The vanishing of $|\boldsymbol{N}(\boldsymbol{k})|$ restores $SO(5)$-symmetry at the Dirac points, which serve as singularities of $\hat{\boldsymbol{N}}(\boldsymbol{k})$. Whether the Dirac points are monopoles of Berry connection, leading to the quantized Berry flux for generic n-fold planes, can only be unambiguously determined by performing second homotopy classification of the gauge group. Since $\pi_2(S^4)$ and $\pi_2(SU(2)) \equiv \pi_2(S^3)$ are trivial, the homotopy analysis of DSMs involves conceptual subtleties, and a physically motivated gauge-fixing procedure of non-Abelian Berry connection is required, which exploits the crystalline symmetries that protect Dirac points. We will show that the form of $\mathcal{C}_n$ operator allows one to identify a pair of global spin-quantization axes that reduces the redundancy of band eigenfunctions from being $Spin(4)$ to $U(1) \times U(1)$, and the gauge-fixed Berry connection admits second homotopy classification.

Model. We substantiate these claims by considering a model of $\mathcal{C}_4$-symmetric, magnetoelectric DSMs, arising from the hybridization between s and p orbitals, *which does not support any gapless surface states*. We will employ the following representation of gamma matrices:

$$\Gamma_{j=1,2,3} = \tau_1 \otimes \sigma_j, \;\; \Gamma_4 = \tau_2 \otimes \sigma_0, \;\; \Gamma_5 = \tau_3 \otimes \sigma_0. \tag{1}$$

The ten commutators $\Gamma_{jl} = [\Gamma_j, \Gamma_l]/(2i)$, with $j = 1, ..., 5$ and $l = 1, ..., 5$ serve as the generators of $SO(5)$ and its double cover group $Spin(5)$. The 2×2 identity matrix τ_0 (σ_0) and the Pauli matrices τ_j's (σ_j's), with $j = 1, 2, 3$ operate on the orbital/parity (spin) index. The relevant $O(5)$ vector is given by

$$\begin{aligned}\boldsymbol{N}(\boldsymbol{k}) = [&t_p \sin k_x, t_p \sin k_y, t_{d,1}(\cos k_x - \cos k_y),\\ &\times\, t_{d,2} \sin k_x \sin k_y, t_s(\Delta - \cos k_x - \cos k_y - \cos k_z)],\end{aligned} \tag{2}$$

where $t_s, t_p, t_{d,1}, t_{d,2}$ are four independent hopping parameters, and the dimensionless parameter Δ controls topological phase transitions. The Hamiltonian is written using the simultaneous eigenstates of Γ_5 and $\mathcal{C}_4$,

$$\begin{aligned}|1\rangle = |+1, e^{i\theta_p}\rangle = \begin{pmatrix}1\\0\\0\\0\end{pmatrix}, |2\rangle = |+1, e^{-i\theta_p}\rangle = \begin{pmatrix}0\\1\\0\\0\end{pmatrix},\\ |3\rangle = |-1, e^{i\theta_q}\rangle = \begin{pmatrix}0\\0\\1\\0\end{pmatrix}, |4\rangle = |-1, e^{-i\theta_q}\rangle = \begin{pmatrix}0\\0\\0\\1\end{pmatrix},\end{aligned} \tag{3}$$

such that

$$\mathcal{C}_4 = e^{i\theta_p\sigma_3} \oplus e^{i\theta_q\sigma_3}, \tag{4}$$

$\theta_p = \frac{\pi}{4}(2p+1)$, with $p = 2 \bmod 4$, $\theta_q = \frac{\pi}{4}(2q+1)$, with $q = 0 \bmod 4$. The $\mathcal{C}_4$ symmetry requires that the Bloch Hamiltonian transforms as $\mathcal{C}_4\hat{H}(\boldsymbol{k})\mathcal{C}_4^\dagger = \hat{H}(\boldsymbol{k}')$, which leads to

$$\begin{aligned}N_1(\boldsymbol{k}') &= \cos(2\theta_+)N_1(\boldsymbol{k}) + \sin(2\theta_+)N_2(\boldsymbol{k}),\\ N_2(\boldsymbol{k}') &= \cos(2\theta_+)N_2(\boldsymbol{k}) - \sin(2\theta_+)N_1(\boldsymbol{k}),\\ N_3(\boldsymbol{k}') &= \cos(2\theta_-)N_3(\boldsymbol{k}) + \sin(2\theta_-)N_4(\boldsymbol{k}),\\ N_4(\boldsymbol{k}') &= \cos(2\theta_-)N_4(\boldsymbol{k}) - \sin(2\theta_-)N_3(\boldsymbol{k}),\\ N_5(\boldsymbol{k}') &= N_5(\boldsymbol{k}),\end{aligned} \tag{5}$$

with $\theta_\pm = \frac{1}{2}(\theta_p \pm \theta_q)$, and the rotated wave vector $(k_x', k_y', k_z') = (-k_y, k_x, k_z)$. The phase diagram is shown in Fig. 1(a). The DSMs ($1 < |\Delta| < 3$) interpolate between trivial insulators ($|\Delta| > 3$) and topological insulators ($|\Delta| < 1$). We will focus on the parameter regime $1 < \Delta < 3$, with the Dirac points located at $\boldsymbol{k}_D = (0, 0, \pm k_D)$, with $\cos(k_D) = (\Delta - 2)$. Away from the high-symmetry locations $k_z = 0, \pi$, the generic fourfold planes of DSMs [3], preserving both $\mathcal{P}$ and $\mathcal{T}$ symmetries display identical form of $\boldsymbol{N}(\boldsymbol{k})$.

For any fixed $|k_z| < k_D$, Eq. (2) describes a two-dimensional insulator, which is topologically equivalent to the system [see Eq. (15)] studied in Ref. [38]. The $O(5)$ vector describes embedding of two distinct $O(3)$ vectors or BHZ models. (i) The BHZ model for $t_{d,1} = t_{d,2} = 0$ supports unit winding number and $U(1)$ spin-conservation law with respect to Γ_{34}, as $[H(t_{d,1} = t_{d,2} = 0), \Gamma_{34}] = 0$. (ii) But

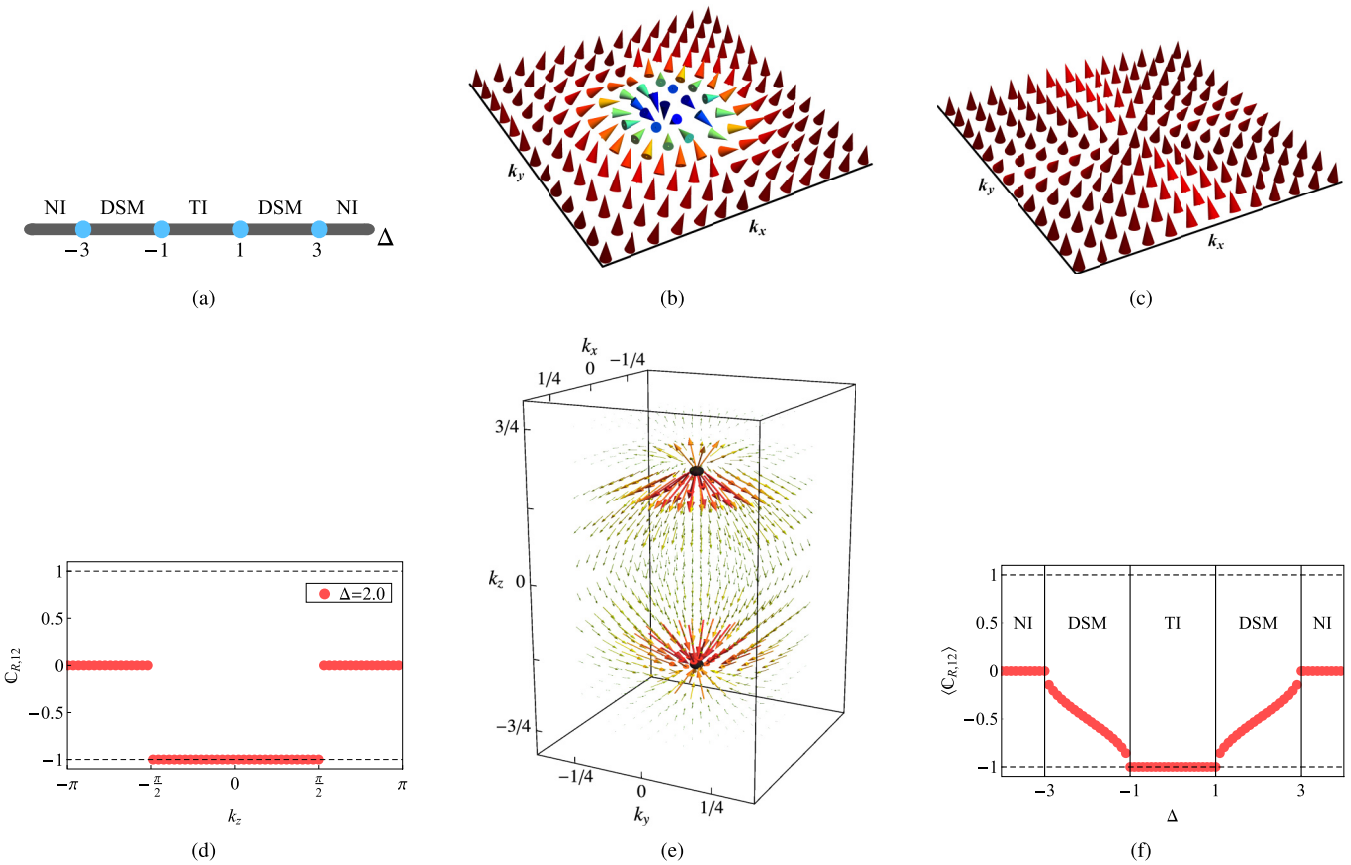

FIG. 1. Phase diagram and bulk topology of Dirac semimetal (DSM) models. (a) Gapless topological phases (DSM), interpolate between a trivial/normal insulator (NI) and a topological insulator (TI), and topologically distinct phases are separated by quantum critical points (blue dots). (b) and (c): For all topologically nontrivial fourfold planes, the three-component, unit vector $\hat{\boldsymbol{n}}_{12}(\hat{\boldsymbol{n}}_{34})$, defined by Eq. (22) displays skyrmion texture with winding number $-1(0)$. (d) The relative Chern number or the quantized flux of $\bar{F}^{12}_{xy}(\boldsymbol{k})$ of Dirac semimetals for $\Delta = 2$. (e) The vector plots of dipole configuration for Abelian projected magnetic fields $B^{12}_i(\boldsymbol{k}) = \frac{1}{2}\epsilon_{ijl}\bar{F}^{12}_{jl}(\boldsymbol{k})$. The momentum components are in units of π. The Dirac points act as a pair of unit strength, $SO(5)$ monopole and antimonopole, where $\mathfrak{C}_{R,12}$ jumps by ± 1. (f) The average value of the relative Chern number $\langle\mathfrak{C}_{R,12}\rangle$ per xy plane, as a function of Δ. Therefore, in contrast to the findings of Ref. [38], our analysis shows that the generic quantum spin Hall insulators described by Eq. (2) support spin Chern number $2 \times \mathfrak{C}_{R,12} = \pm 2$.

the BHZ model for $t_p = 0$, exhibits double winding number, and $U(1)$ spin-conservation law with respect to Γ_{12}, as $[H(t_p = 0), \Gamma_{12}] = 0$. When studied separately, they support one and two pairs of gapless, helical edge modes, respectively. The generic Bloch Hamiltonian lacks such global $U(1)$ spin-rotation symmetries, as $[H, \Gamma_{12}] \neq 0$ and $[H, \Gamma_{34}] \neq 0$, and does not support gapless edge states. Therefore, we outline the formalism for computing Berry curvatures for generic model.

Berry curvature. The $\mathcal{PT}$ symmetry is implemented by $\Gamma_{24}\hat{H}^*(\boldsymbol{k})\Gamma_{24} = \hat{H}(\boldsymbol{k})$, and the diagonalizing matrix $U(\boldsymbol{k})$ must satisfy the constraints

$$U^\dagger(\boldsymbol{k})\hat{H}(\boldsymbol{k})U(\boldsymbol{k}) = |\boldsymbol{N}(\boldsymbol{k})|\Gamma_5, \tag{6}$$

$$U^\dagger(\boldsymbol{k})\Gamma_{24}U^*(\boldsymbol{k}) = \Gamma_{24}. \tag{7}$$

Hence, $U(\boldsymbol{k})$ has the general form [42,43],

$$U(\boldsymbol{k}) = \begin{bmatrix} \cos\frac{\theta(\boldsymbol{k})}{2}g_+(\boldsymbol{k}) & i\sin\frac{\theta(\boldsymbol{k})}{2}u(\boldsymbol{k})g_-(\boldsymbol{k}) \\ i\sin\frac{\theta(\boldsymbol{k})}{2}u^\dagger(\boldsymbol{k})g_+(\boldsymbol{k}) & \cos\frac{\theta(\boldsymbol{k})}{2}g_-(\boldsymbol{k}) \end{bmatrix}, \tag{8}$$

where

$$\cos[\theta(\boldsymbol{k})] = \frac{N_5(\boldsymbol{k})}{|\boldsymbol{N}(\boldsymbol{k})|}, \tag{9}$$

$$u(\boldsymbol{k}) = \frac{N_4(\boldsymbol{k})\sigma_0 + i\sum_{j=1}^{3} N_j(\boldsymbol{k})\sigma_j}{\sqrt{N_1^2(\boldsymbol{k}) + N_2^2(\boldsymbol{k}) + N_3^2(\boldsymbol{k}) + N_4^2(\boldsymbol{k})}}. \tag{10}$$

The first (last) two columns correspond to the eigenfunctions of conduction (valence) bands, the $SU(2)$ matrix $u(\boldsymbol{k})$ describes hybridization between two orbitals, and the $SU(2)$ matrices $g_\pm(\boldsymbol{k})$ describe gauge freedom in selecting the eigenfunctions for conduction and valence bands, respectively. Owing to the transformation properties of $\boldsymbol{N}(\boldsymbol{k})$ under $\mathcal{C}_4$ rotation [(see Eq. (5)],

$$u(\boldsymbol{k}') = e^{i\theta_p\sigma_3}u(\boldsymbol{k})e^{-i\theta_q\sigma_3}. \tag{11}$$

From $U(\boldsymbol{k})$ one finds the following intraband $SU(2)$ connections:

$$\boldsymbol{A}_+(\boldsymbol{k}) = \sin^2\frac{\theta}{2}\, g_+^\dagger[-iu\nabla u^\dagger]g_+ - ig_+^\dagger\nabla g_+,$$
$$\boldsymbol{A}_-(\boldsymbol{k}) = \sin^2\frac{\theta}{2}\, g_-^\dagger[-iu^\dagger\nabla u]g_- - ig_-^\dagger\nabla g_-, \quad (12)$$

for the conduction and valence bands, respectively. For notational compactness, we have suppressed the explicit $\boldsymbol{k}$ dependence of θ, u, and $g_\pm$.

Since the $\mathcal{C}_4$ symmetry leads to the constraint

$$[U^\dagger(\boldsymbol{k}')\mathcal{C}_4U(\boldsymbol{k}), \Gamma_5] = 0, \quad (13)$$

the transformed rotation operator or the sewing matrix $\mathcal{C}_4'(\boldsymbol{k}) \equiv U^\dagger(\boldsymbol{k}')\mathcal{C}_4U(\boldsymbol{k})$ acquires the form

$$\mathcal{C}_4'(\boldsymbol{k}) = [g_+^\dagger(\boldsymbol{k}')e^{i\theta_p\sigma_3}g_+(\boldsymbol{k})] \oplus [g_-^\dagger(\boldsymbol{k}')e^{i\theta_q\sigma_3}g_-(\boldsymbol{k})]. \quad (14)$$

Notice that the gauge choice $g_\pm(\boldsymbol{k}) = e^{i\alpha_\pm(\boldsymbol{k})\sigma_3}$ keeps the spin quantization axes unaffected, and the sewing matrix reduces to the global $\mathcal{C}_4$ operator.

Any general choice of gauge specify a pair of local spin quantization axes $\hat{\boldsymbol{m}}_\pm(\boldsymbol{k})$, according to $g_\pm^\dagger(\boldsymbol{k})\sigma_3 g_\pm(\boldsymbol{k}) = \hat{\boldsymbol{m}}_\pm(\boldsymbol{k})\cdot\boldsymbol{\sigma}$. Once $g_\pm(\boldsymbol{k})$ are identified, $U(\boldsymbol{k})$ only exhibits residual $U(1)\times U(1)$ gauge freedom, corresponding to the spin rotations about $\hat{\boldsymbol{m}}_\pm(\boldsymbol{k})$, i.e., $g_\pm(\boldsymbol{k}) \to g_\pm(\boldsymbol{k})\exp[i\varphi_\pm(\boldsymbol{k})\hat{\boldsymbol{m}}_\pm(\boldsymbol{k})\cdot\boldsymbol{\sigma}]$. Consequently, the gauge group of intraband Berry connection is given by $Spin(4)/[U(1)\times U(1)]$, with the second homotopy class

$$\pi_2\left(\frac{Spin(4)}{U(1)\times U(1)}\right) = \pi_1(U(1)\times U(1)) = \mathbb{Z}\times\mathbb{Z}. \quad (15)$$

Hence, the topology of fourfold planes and the Dirac points are governed by a pair of integer invariants, and *the Dirac points can be identified as non-Abelian monopoles. The analysis of $\mathcal{C}_{n=3,6}$ fold symmetric DSMs can be performed using this formalism, after setting* $\theta_p = \frac{\pi}{n}(2p+1)$, with $p = 0, .., n-1 \bmod n$, $\theta_q = \frac{\pi}{n}(2q+1)$, with $p = 0, .., n-1 \bmod n$, and $\boldsymbol{k}' = (k_x\cos(2\pi/n) - k_y\sin(2\pi/n), -k_x\cos(2\pi/n) + k_y\cos(2\pi/n), k_z)$.

The Abelian projected Berry connections can be obtained as $\bar{\boldsymbol{A}}_\pm(\boldsymbol{k}) = \frac{1}{2}Tr[\boldsymbol{A}_\pm(\boldsymbol{k})\hat{\boldsymbol{m}}_\pm(\boldsymbol{k})\cdot\boldsymbol{\sigma}] = \frac{1}{2}Tr[\boldsymbol{A}_\pm(\boldsymbol{k})\, g_\pm^\dagger(\boldsymbol{k})\sigma_3 g_\pm(\boldsymbol{k})]$, leading to

$$\bar{\boldsymbol{A}}_+(\boldsymbol{k}) = \frac{1}{2}\sin^2\frac{\theta}{2}\, Tr[-iu\nabla u^\dagger\sigma_3] + \frac{i}{2}Tr[g_+\nabla g_+^\dagger\sigma_3],$$
$$\bar{\boldsymbol{A}}_-(\boldsymbol{k}) = \frac{1}{2}\sin^2\frac{\theta}{2}\, Tr[-iu^\dagger\nabla u\sigma_3] + \frac{i}{2}Tr[g_-\,\nabla g_-^\dagger\sigma_3]. \quad (16)$$

Consequently, the gauge-invariant, quantized Berry flux can be determined from the Abelian field strength tensors (or Berry curvatures) $\bar{F}_{ij,\pm}(\boldsymbol{k}) = \partial_i\bar{A}_{j,\pm}(\boldsymbol{k}) - \partial_j\bar{A}_{i,\pm}(\boldsymbol{k})$. For all smooth gauge transformations, such that the spin-quantization vectors $\hat{\boldsymbol{m}}(\boldsymbol{k})$ are topologically trivial (meaning the gauge-fixing operators $\hat{\boldsymbol{m}}_\pm(\boldsymbol{k})\cdot\boldsymbol{\sigma}$ do not correspond to fictitious two-band models of Chern insulators), $i/2Tr[g_\pm\nabla g_\pm^\dagger\sigma_3]$ terms cannot contribute to the quantized flux of $\bar{F}_{ij,\pm}(\boldsymbol{k})$ or the relative Chern numbers for 4-fold planes, defined as

$$\mathfrak{C}_{R,\pm}(k_z) = \frac{1}{2\pi}\int_{T^2} dk_x dk_y\, \bar{F}_{xy,\pm}(\boldsymbol{k}). \quad (17)$$

To compare against the spin-Chern number of Ref. [38], we have to trace over the Kramers index of occupied bands (i.e., trace over σ_3). Hence, $C_s = 2\mathfrak{C}_{R,-}$.

Quantized Berry flux. Next we perform explicit analytical calculations of Berry flux with the global gauge choice $g_\pm(\boldsymbol{k}) = \sigma_0$, corresponding to the spin quantization axes $\hat{\boldsymbol{m}}_\pm(\boldsymbol{k}) = (0,0,1)$. This choice implies that the conduction and valence band eigenfunctions are obtained by operating with projectors on the global basis:

$$|+;\uparrow\rangle = \frac{\hat{P}_+|1\rangle}{\sqrt{\langle 1|\hat{P}_+|1\rangle}}, |+;\downarrow\rangle = \frac{\hat{P}_+|2\rangle}{\sqrt{\langle 2|\hat{P}_+|2\rangle}},$$
$$|-;\uparrow\rangle = \frac{\hat{P}_-|3\rangle}{\sqrt{\langle 3|\hat{P}_-|3\rangle}}, |-;\downarrow\rangle = \frac{\hat{P}_-|4\rangle}{\sqrt{\langle 4|\hat{P}_-|4\rangle}}. \quad (18)$$

Therefore, the expressions for Berry curvatures only involve the matrix elements of $\hat{H}(\boldsymbol{k})$. It is convenient to define symmetric and anti-symmetric combinations of Berry curvatures as $\bar{F}_{\rm ij}^{12} = (\bar{F}_{\rm ij,+} + \bar{F}_{\rm ij,-})/2$, and $\bar{F}_{\rm ij}^{34} = (\bar{F}_{\rm ij,+} - \bar{F}_{\rm ij,-})/2$. These curvatures will be associated with the diagonal, Cartan generators of $SO(5)$ group, namely $\Gamma_{12} = \tau_0\otimes\sigma_3$ and $\Gamma_{34} = \tau_3\otimes\sigma_3$, and can be elegantly written as

$$\bar{F}_{ij}^{ab} = \sin(\theta_{ab})[\partial_i\theta_{ab}\partial_j\phi_{ab} - \partial_j\theta_{ab}\partial_i\phi_{ab}], \quad (19)$$

where we have introduced two sets of spherical polar angles $(\theta_{12}(\boldsymbol{k}), \phi_{12}(\boldsymbol{k}))$ and $(\theta_{34}(\boldsymbol{k}), \phi_{34}(\boldsymbol{k}))$, such that

$$\tan[\phi_{ab}(\boldsymbol{k})] = \frac{N_b(\boldsymbol{k})}{N_a(\boldsymbol{k})}, \quad (20)$$

$$\cos[\theta_{ab}(\boldsymbol{k})] = 1 - \frac{\left[N_a^2(\boldsymbol{k}) + N_b^2(\boldsymbol{k})\right]}{|\boldsymbol{N}(\boldsymbol{k})|[|\boldsymbol{N}(\boldsymbol{k})| + N_5(\boldsymbol{k})]}. \quad (21)$$

The quantized flux of $\bar{F}_{ij}^{12}$ and $\bar{F}_{ij}^{34}$ can only exist if the BZ two-torus can wrap around unit two spheres, defined by

$$\hat{\mathbf{n}}_{ab} = (\sin\theta_{ab}\cos\phi_{ab}, \sin\theta_{ab}\sin\phi_{ab}, \cos\theta_{ab}). \quad (22)$$

Notice that $\Phi_{xy}^{12}(k_z) = 2\pi\,\mathfrak{C}_{R,12}(k_z)$ and $\Phi_{xy}^{34}(k_z) = 2\pi\,\mathfrak{C}_{R,34}(k_z)$ describe the flux of Abelian fields $\bar{F}^{12}$ and $\bar{F}^{34}$, respectively.

For all topologically nontrivial fourfold planes of $\mathcal{C}_4$-symmetric DSMs described by Eq. (2), only θ_{12} interpolates between 0 and π, leading to the skyrmion configuration for the unit vector $\hat{\boldsymbol{n}}_{12}$, as shown in Fig. 1(b). In contrast to this, θ_{34} does not interpolate between 0 and π, and the corresponding unit vector $\hat{\boldsymbol{n}}_{34}$ is topologically trivial, as shown in Fig. 1(c). The quantization of the relative Chern numbers, and their discontinuities at the Dirac points are shown in Fig. 1(d). The monopole numbers for the Dirac points at $\boldsymbol{k} = (0,0,\pm k_{D,j})$ are determined by

$$\mathcal{N}_{12}(\pm k_{D,j}) = \lim_{\epsilon\to 0}[\mathfrak{C}_{R,12}(k_z = \pm k_{D,j} + \epsilon) - \mathfrak{C}_{R,12}(k_z = \pm k_{D,j} - \epsilon)] = \pm 1, \quad (23)$$
$$\mathcal{N}_{34}(\pm k_{D,j}) = 0. \quad (24)$$

In Fig. 1(e), we illustrate the structure of Abelian projected magnetic fields $B_i^{12}(\boldsymbol{k}) = \frac{1}{2}\epsilon_{ijl}\bar{F}_{jl}^{12}(\boldsymbol{k})$, which support dipole configuration. Using the k_z-dependent relative Chern numbers, we can also define the average relative Chern numbers per xy plane $\langle\mathfrak{C}_{R,ab}\rangle(\Delta) = \frac{1}{2\pi}\int_{-\pi}^{\pi} dk_z\, \mathfrak{C}_{R,ab}(k_z)$, which is

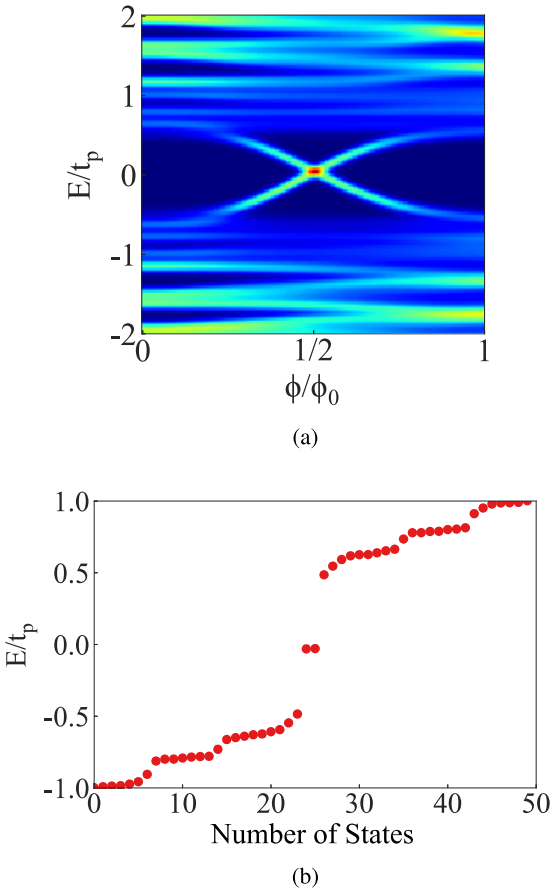

FIG. 2. Spin-charge separation and spin-pumping for nontrivial planes of Dirac semimetals. (a) Local density of states for magnetic flux tube, as a function of energy E (measured in units of hopping parameter t_p) and the strength of flux ϕ, and $\phi_0 = h/e$ is the flux quantum. (b) The number of states vs energy eigenvalues for $\phi = \phi_0/2$, showing the higher-order topological insulators, described by Eq. (2) support twofold degenerate, zero-energy states. As ϕ is tuned from 0 to ϕ_0, one Kramers pair is pumped. If the relative (spin) Chern number was ± 2 (± 4), two Kramers pair would be pumped, and π flux tube would bind four zero-energy, midgap states.

shown in Fig. 1(f). Therefore, our results correspond to spin Chern number ± 2 instead of ± 4. We note that the stacked BHZ model with $t_{d,1} = t_{d,2} = 0$, the stacked HOTI with $t_{d,2} = 0$ [36], and the stacked HOTI with $t_{d,1} = 0$ support identical quantized flux of $\bar{F}^{12}_{jl}(\boldsymbol{k})$. Hence, the relative Chern number acts as a topological order parameter for various phases, controlling the strength of generalized QSH effect, which can be seen in the following manner.

Generalized QSH effect. References [44–47] have identified spin-charge separation as the nonperturbative signature of QSH, which can survive as a genuine topological response even in the absence of $U(1)$ spin conservation law. For the BHZ model ($t_{d,1/2} = 0$) and closely related Z_2 FOTI, supporting gapless edge modes, it was shown that a magnetic π-flux tube binds twofold degenerate, zero-energy, midgap states. When both bound modes are occupied (empty), the spin or Kramers-singlet state carries charge $+e$ ($-e$). In contrast to this, the half-filling of bound modes corresponds to spin or Kramers-doublet with charge $e = 0$. When the strength of flux is varied adiabatically between 0 and full flux quantum $\phi_0 = h/e$, ground state carrying unit relative Chern number (spin Chern number ± 2) shows pumping of spin or one Kramers pair.

To demonstrate spin-charge separation and spin-pumping for $\mathcal{C}_4$-symmetric HOTI, we have computed the local density of states in the presence of a magnetic flux tube, oriented along z axis, for a system size 21×21, under periodic boundary condition. The local density of states for flux tube is shown in Fig. 2(a) as a function of energy and the strength of flux ϕ. The calculations were performed with hopping parameters $t_s = t_p = t_{d,1} = t_{d,2}$, $k_z = \pi/2$, and $\Delta = 1.5$. The low-energy states for $\phi = \phi_0/2$ or π flux are shown in Fig. 2(b), providing clear evidence for the existence of two-fold degenerate, midgap states at zero energy, and pumping of one Kramers pair, when ϕ is tuned from 0 to ϕ_0. All topologically nontrivial planes of DSMs can support such midgap states (which may or may not be at zero energy), and their total number corresponds to $\Delta k_D/\pi$.

In conclusion, we have provided second homotopy classification of generic fourfold planes and Dirac points. We have shown that generic planes are generalized QSH insulators, possessing relative (spin) Chern number ± 1 (± 2). The combined analysis of non-Abelian Berry flux in momentum space and real-space topological response described in this work is widely applicable for studying first- and higher-order topological insulators and semimetals. This is a unified theoretical framework that is capable of addressing complex band structures of analytically known effective models [48–50] and numerical tight-binding models [49,51], for which the presence of quantized Berry flux cannot be easily inferred from simple symmetry-based indicators.

Acknowledgments. This work was supported by the National Science Foundation MRSEC program (DMR-1720139) at the Materials Research Center of Northwestern University, and the start up funds of P.G. provided by the Northwestern University. P.G. completed a part of this work at the Aspen Center For Physics, which is supported by National Science Foundation Grant No. PHY-1607611. D.P. and J.M.R. acknowledge the Army Research Office under Grant No. W911NF-15-1-0017 for financial support and the DOD-HPCMP for computational resources.

[1] Z. Wang, Y. Sun, X.-Q. Chen, C. Franchini, G. Xu, H. Weng, X. Dai, and Z. Fang, Dirac semimetal and topological phase transitions in A_3Bi (A = Na, K, Rb), Phys. Rev. B **85**, 195320 (2012).

[2] Z. Wang, H. Weng, Q. Wu, X. Dai, and Z. Fang, Three-dimensional Dirac semimetal and quantum transport in Cd_3As_2, Phys. Rev. B **88**, 125427 (2013).

[3] B.-J. Yang and N. Nagaosa, Classification of stable three-dimensional Dirac semimetals with nontrivial topology, Nat. Commun. **5**, 4898 (2014).

[4] B.-J. Yang, T. Morimoto, and A. Furusaki, Topological charges of three-dimensional Dirac semimetals with rotation symmetry, Phys. Rev. B **92**, 165120 (2015).

[5] E. V. Gorbar, V. A. Miransky, I. A. Shovkovy, and P. O. Sukhachov, Dirac semimetals $A_3Bi(a = Na, K, Rb)$ as Z_2Weyl semimetals, Phys. Rev. B **91**, 121101(R) (2015).

[6] A. A. Burkov and Y. B. Kim, Z_2 and Chiral Anomalies in Topological Dirac Semimetals, Phys. Rev. Lett. **117**, 136602 (2016).

[7] M. Kargarian, M. Randeria, and Y.-M. Lu, Are the surface Fermi arcs in Dirac semimetals topologically protected? Proc. Natl. Acad. Sci. USA **113**, 8648 (2016).

[8] Z. Gao, M. Hua, H. Zhang, and X. Zhang, Classification of stable Dirac and Weyl semimetals with reflection and rotational symmetry, Phys. Rev. B **93**, 205109 (2016).

[9] P. Tang, Q. Zhou, G. Xu, and S.-C. Zhang, DiracFermions in an antiferromagnetic semimetal, Nat. Phys. **12**, 1100 (2016).

[10] C.-K. Chiu, J. C.Y. Teo, A.P. Schnyder, and S. Ryu, Classification of topological quantum matter with symmetries, Rev. Mod. Phys. **88**, 035005 (2016).

[11] T.-R. Chang, S.-Y. Xu, D. S. Sanchez, W.-F. Tsai, S.-M. Huang, G. Chang, C.-H. Hsu, G. Bian *et al.*, Type-II Symmetry-Protected Topological Dirac Semimetals, Phys. Rev. Lett. **119**, 026404 (2017).

[12] C. Le, S. Qin, X. Wu, X. Dai, P. Fu, C. Fang, and J. Hu, Three-dimensional topological critical Dirac semimetal in AMgBi(A = K, Rb, Cs), Phys. Rev. B **96**, 115121 (2017).

[13] C. Le, X. Wu, S. Qin, Y. Li, R. Thomale, F.-C. Zhang, and J. Hu, Dirac semimetal in β-CuI without surface Fermi arcs, Proc. Natl. Acad. Sci. USA **115**, 8311 (2018).

[14] M. Kargarian, Y.-M. Lu, and M. Randeria, Deformation and stability of surface states in Dirac semimetals, Phys. Rev. B **97**, 165129 (2018).

[15] N.P. Armitage, E.J. Mele, and A. Vishwanath, Weyl and Dirac semimetals in three-dimensional solids, Rev. Mod. Phys. **90**, 015001 (2018).

[16] R. Kim, B.-J. Yang, and C. H. Kim, Crystalline topological Dirac semimetal phase in rutile structure β'-PtO_2, Phys. Rev. B **99**, 045130 (2019).

[17] M. Lin and T.L. Hughes, Topological quadrupolar semimetals, Phys. Rev. B **98**, 241103(R) (2018).

[18] A. L. Szabó, R. Moessner, and B. Roy, Strain-engineered higher-order topological phases for spin$-3/2$ Luttinger Fermions, Phys. Rev. B **101**, 121301(R) (2020).

[19] B. J. Wieder, Z. Wang, J. Cano, X. Dai, L. M. Schoop, B. Bradlyn, and B. A. Bernevig, Strong and fragile topological Dirac semimetals with higher-order Fermi arcs, Nat. Commun. **11**, 627 (2020).

[20] Z. K. Liu, B. Zhou, Y. Zhang, Z. J. Wang, H. M. Weng, D. Prabhakaran, S.-K. Mo, Z. X. Shen *et al.*, Discovery of a three-dimensional topological Dirac semimetal, Na_3Bi, Science **343**, 864 (2014).

[21] J. Xiong, S. K. Kushwaha, T. Liang, J. W. Krizan, M. Hirschberger, W. Wang, R. J. Cava, and N. P. Ong, Evidence for the chiral anomaly in the Dirac semimetal Na_3Bi, Science **350**, 413 (2015).

[22] S. K Kushwaha, J. W Krizan, B. E. Feldman, A. Gyenis, M. T. Randeria, J. Xiong, S.-Y. Xu, N. Alidoust *et al.*, Bulk crystal growth and electronic characterization of the 3d Dirac semimetal Na_3Bi, APL Mater. **3**, 041504 (2015).

[23] A. Liang, C. Chen, Z. Wang, Y. Shi, Y. Feng, H. Yi, Z. Xie, S. He *et al.*, Electronic structure, Dirac points and Fermi arc surface states in three-dimensional Dirac semimetal Na_3Bi from angle-resolved photoemission spectroscopy, Chinese Phys. B **25**, 077101 (2016).

[24] Z.K. Liu, J. Jiang, B. Zhou, Z.J. Wang, Y. Zhang, H.M. Weng, D. Prabhakaran, S.K. Mo *et al.*, A stable three-dimensional topological Dirac semimetal Cd_3As_2, Nat. Mater. **13**, 677 (2014).

[25] M. Neupane, S.-Y. Xu, R. Sankar, N. Alidoust, G. Bian, C. Liu, I. Belopolski, T.-R. Chang *et al.*, Observation of a three-dimensional topological Dirac semimetal phase in high-mobility Cd_3As_2, Nat. Commun. **5**, 1 (2014).

[26] L.P. He, X.C. Hong, J.K. Dong, J. Pan, Z. Zhang, J. Zhang, and S.Y. Li, Quantum Transport Evidence for the Three-Dimensional Dirac Semimetal Phase in Cd_3As_2, Phys. Rev. Lett. **113**, 246402 (2014).

[27] S. Borisenko, Q. Gibson, D. Evtushinsky, V. Zabolotnyy, B. Büchner, and R. J. Cava, Experimental Realization of a Three-Dimensional Dirac Semimetal, Phys. Rev. Lett. **113**, 027603 (2014).

[28] P. J.W. Moll, N. L. Nair, T. Helm, A. C. Potter, I. Kimchi, A. Vishwanath, and J. G. Analytis, Transport evidence for Fermi-arc-mediated chirality transfer in the Dirac semimetal Cd_3As_2, Nature (London) **535**, 266 (2016).

[29] S. Jeon, B. B. Zhou, A. Gyenis, B. E. Feldman, I. Kimchi, A. C. Potter, Q. D. Gibson, R. J. Cava *et al.*, Landau quantization and quasiparticle interference in the three-dimensional Dirac semimetal Cd_3As_2, Nat. Mater. **13**, 851 (2014).

[30] H.-J. Noh, J. Jeong, E.-J. Cho, K. Kim, B. I. Min, and B.G. Park, Experimental Realization of Type-II DiracFermions in a $PdTe_2$ Superconductor, Phys. Rev. Lett. **119**, 016401 (2017).

[31] Y. Wu, N. H. Jo, L.-L. Wang, C. A. Schmidt, K. M. Neilson, B. Schrunk, P. Swatek, A. Eaton *et al.*, Fragility of Fermi arcs in Dirac semimetals, Phys. Rev. B **99**, 161113(R) (2019).

[32] Z. Lin, C. Wang, P. Wang, S. Yi, L. Li, Q. Zhang, Y. Wang, Z. Wang, H. Huang, Y. Sun *et al.*, DiracFermions in antiferromagnetic FeSn kagome lattices with combined space inversion and time-reversal symmetry, Phys. Rev. B **102**, 155103 (2020).

[33] B.A. Bernevig, T.L. Hughes, and S.-C. Zhang, Quantum spin hall effect and topological phase transition in HgTe quantum wells, Science **314**, 1757 (2006).

[34] C. L. Kane and E. J. Mele, Z_2 Topological Order and the Quantum Spin Hall Effect, Phys. Rev. Lett. **95**, 146802 (2005).

[35] Y. Fang and J. Cano, Classification of Dirac points with higher-order Fermi arcs, Phys. Rev. B **104**, 245101 (2021).

[36] W. A Benalcazar, B.A. Bernevig, and T.L. Hughes, Quantized electric multipole insulators, Science **357**, 61 (2017).

[37] D. N. Sheng, Z. Y. Weng, L. Sheng, and F. D. M. Haldane, Quantum Spin-Hall Effect and Topologically Invariant Chern Numbers, Phys. Rev. Lett. **97**, 036808 (2006).

[38] X.-L. Qi, Y.-S. Wu, and S.-C. Zhang, General theorem relating the bulk topological number to edge states in two-dimensional insulators, Phys. Rev. B **74**, 045125 (2006).

[39] Z.-D. Song, L. Elcoro, and B.A. Bernevig, Twisted bulk-boundary correspondence of fragile topology, Science **367**, 794 (2020).

[40] J. E. Avron, L. Sadun, J. Segert, and B. Simon, Topological Invariants in Fermi Systems with Time-Reversal Invariance, Phys. Rev. Lett. **61**, 1329 (1988).

[41] J.E. Avron, L. Sadun, J. Segert, and B. Simon, Chern numbers, quaternions, and Berry's phases in Fermi systems, Commun. Math. Phys. **124**, 595 (1989).

[42] E. Demler and S.-C. Zhang, Non-abelian holonomy of BCS and SDW quasiparticles, Ann. Phys. **271**, 83 (1999).

[43] S. Murakami, N. Nagaosa, and S.-C. Zhang, SU(2) non-Abelian holonomy and dissipationless spin current in semiconductors, Phys. Rev. B **69**, 235206 (2004).

[44] X.-L. Qi and S.-C. Zhang, Spin-Charge Separation in the Quantum Spin Hall State, Phys. Rev. Lett. **101**, 086802 (2008).

[45] Y. Ran, A. Vishwanath, and D.-H. Lee, Spin-Charge Separated Solitons in a Topological Band Insulator, Phys. Rev. Lett. **101**, 086801 (2008).

[46] V. Juričić, A. Mesaros, R.-J. Slager, and J. Zaanen, Universal Probes of Two-Dimensional Topological Insulators: Dislocation and π Flux, Phys. Rev. Lett. **108**, 106403 (2012).

[47] A. Mesaros, R.-J. Slager, J. Zaanen, and V. Juričić, Zero-energy states bound to a magnetic π-flux vortex in a two-dimensional topological insulator, Nucl. Phys. B **867**, 977 (2013).

[48] S. Sur, A. C. Tyner, and P. Goswami, Mixed-order topology of Benalcazar-Bernevig-Hughes models, arXiv:2201.07205 (2022).

[49] A. C. Tyner and P. Goswami, Symmetry indicators vs. bulk winding numbers of topologically non-trivial bands, arXiv:2109.06871 (2021).

[50] A. C. Tyner and P. Goswami, Witten effect and $\mathbb{Z}$-classification of three-dimensional topological insulators, arXiv:2206.10636 (2022).

[51] A. C. Tyner and P. Goswami, Spin-charge separation and quantum spin hall effect of β-bismuthene, arXiv:2209.13582 (2022).